FOOD AND BIOPRODUCTS PROCESSING 99 (2016) 38–50

Contents lists available at ScienceDirect

Food and Bioproducts Processing

journal homepage: www.elsevier.com/locate/fbp

Self-drainage of viscous liquids in vertical and inclined pipes

A. Ali, A. Underwood, Y.-R. Lee, D.I. Wilson*

Department of Chemical Engineering and Biotechnology, New Museums Site, Pembroke Street, Cambridge CB2 3RA, UK

ARTICLE INFO

Article history:
Received 27 August 2015
Received in revised form 13 March 2016
Accepted 17 March 2016
Available online 26 March 2016

Keywords:
Cleaning
Drainage
Fluid mechanics
Laminar
Shear-thinning
Thixotropy

ABSTRACT

The rate of drainage of a viscous liquid from initially full cylindrical tubes inclined at various angles to the vertical (0°, 30°, 45° and 60°) was studied in glass and polymethylmethacrylate (Perspex™) tubes of various lengths and diameters using three food materials: honey (Newtonian) and two variants of Marmite™ spread (both exhibiting complex rheological behaviour, including shear-thinning and thixotropy). The behaviour was marked by an initially steady rate of drainage in which an air slug descended the tube, followed by slower drainage from an annular film remaining on the wall. Eventually the liquid stopped draining as a filament and entered a dripping regime. Drainage was insensitive to the tube material, whereas the stages of drainage were influenced by the geometry and angle of inclination. Quantitative models are presented for the rate and extent of the initial drainage stage, the rate in a second linear stage (where it existed), and the rate of drainage in the third, falling rate stage. The fourth and final stage, characterised by drop formation, was not modelled. The initial rate can be predicted with reasonable accuracy, allowing the time to remove approximately 50% of the material in a short waiting phase to be calculated, *e.g.* $t = 8\nu L/R^2 g$ for a Newtonian liquid with kinematic viscosity ν in a vertical pipe of radius R and length L. The agreement with the other models is less exact but they capture the general trends reasonably.

1. Introduction

Viscous liquids are widely used in food processing. Products such as sauces and spreads (*e.g.* Marmite™, White et al., 2008) are manufactured and sold as viscous, non-Newtonian liquids. Others such as ice cream and chocolate (*e.g.* Taylor et al., 2009) are processed as non-Newtonian fluids but sold as solids, while other products employ viscous liquids as components in their assembly, *e.g.* chocolate for coating, jams and syrups for filling. Food processing operations regularly require the lines carrying these viscous liquids to be cleared, either as part of shutdown for maintenance, changeover to a different batch, or for cleaning and disinfection. This is often achieved by recirculating water as part of a cleaning-in-place cycle. The water initially pushes out a central core of material and the surrounding annulus is subsequently eroded by the shear stress imposed by the water flow (Mickaily and Middleman, 1993; Palabiyik et al., 2014; Fan et al., 2015), aided by dissolution if the material is soluble. Water flushing can be fast but causes product loss and generation of large volumes of contaminated water, which must be treated.

An alternative approach is to allow the material to drain back to a reservoir under the action of gravity. This will extend the time required to clear the line and will still need to be followed by a water flush to complete the operation, but will reduce product loss and water consumption. There will be an optimal time to start flushing, which will be determined by the amount of material remaining in a line over time. This is

* *Corresponding author*. Tel.: +44 1223 334791; fax: +44 1223 334796.
E-mail address: diw11@cam.ac.uk (D.I. Wilson).
http://dx.doi.org/10.1016/j.fbp.2016.03.005

Nomenclature

Roman

a_1	constant, after Eq. (23), $m^{2-\alpha}\,s^{-1}$
a_2	constant, Eq. (23), $m^{2+1/\alpha}\,s^{-1/\alpha}$
a_3	constant, Eq. (24), $m^3\,s^{-(1+\beta)}$
D	tube diameter, m
Eo	Eötvös number, –
g	acceleration due to gravity, $m\,s^{-2}$
k	constant, Eq. (21), $m^{2-\alpha}\,s^{-1}$
K	consistency, power law fluid, $Pa\,s^n$
L	tube length, m
$\dot{m}$	mass flow rate, $g\,s^{-1}$
$\dot{m}_{pred}$	predicted mass flow rate, $g\,s^{-1}$
m	Mass of liquid in tube, g
m^*	Fraction of liquid remaining in tube at end of stage I, –
m_0, m_i	Mass of liquid initially, at time t_i, g
n	Power law index, Eq. (6), –
Q_A	Flow rate in annulus, $m^3\,s^{-1}$
Q_i	Flow rate, stage i, $m^3\,s^{-1}$
Q_N	Flow rate in annulus, Nusselt approximation, $m^3\,s^{-1}$
$Q_{I,PL}$	Flow rate in stage I, power law fluid, $m^3\,s^{-1}$
R	tube radius, m
r	radial co-ordinate, m
r_i	radial position of annulus interface, m
Re	Reynolds number, –
T	temperature, K
t	time, s
t'	elapsed time in stage III, s
t_i	time at end of stage i, s
u, u_i	velocity in annulus, velocity at interface, $m\,s^{-1}$
U	mean velocity of liquid, $m\,s^{-1}$
U_s	velocity of slug front, $m\,s^{-1}$
V_A	volume of annulus, m^3
x	dimensionless radius, $x = r/R$, –
z	axial co-ordinate, m

Greek

α	power law index, Eq. (20), –
β	power law index, Eq. (24), –
γ	film thickness, m
$\dot{\gamma}_{app}$	apparent shear rate, s^{-1}
μ	dynamic viscosity, Pa s
θ	angle of inclination from vertical, –
ρ	density, $kg\,m^{-3}$
σ	surface tension, $N\,m^{-1}$
τ	shear stress, Pa
τ_w	wall shear stress, Pa
ν	kinematic viscosity, $m^2\,s^{-1}$

a transient fluid flow problem which does not appear to have received much attention in the literature, and particularly for viscous, non-Newtonian liquids which are commonly encountered in the food sector (see Loibl et al., 2012). The amount of product wasted can be considerable: for example, Cragnell et al. (2014) reported that 5–10% of fermented milk products are left behind on packaging surfaces when the consumer decants the contents from a carton.

We report a series of experiments where a transparent tube, initially full of viscous liquid and open at the top, is allowed to discharge from the open lower end under the action of gravity. As liquid drains, air enters from the top in the form of a long slug which descends at velocity U_s, leaving an annular film behind on the tube wall (see Fig. 1). Drainage behaviour was studied for a series of glass and polymethylmethacrylate (Perspex) pipes of different lengths and diameters. Three liquids were studied: a commercial honey and two varieties of Marmite™, all of which are viscous food fluids. Whereas the former is Newtonian, Marmite™ is a complex fluid, being a concentrated suspension of protein fragments from brewer's yeast in a highly saline solution. It exhibits shear-thinning behaviour and thixotropy, with an apparent memory of recent shear history (White et al., 2008). The two varieties studied here differed in solids content and rheology.

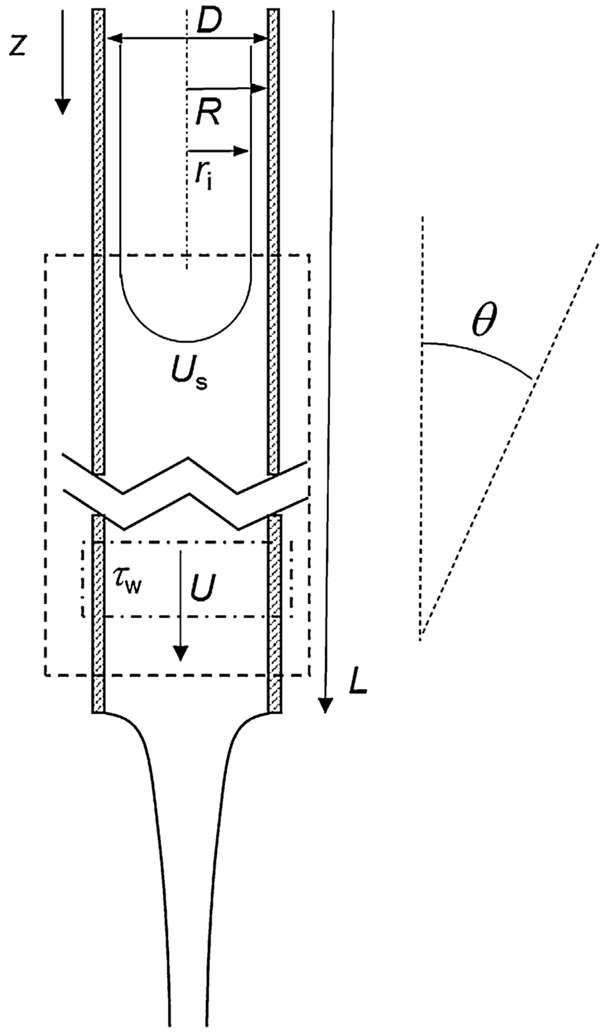

Fig. 1 – Schematic of flow from a draining tube in region I. A slug of air moves downwards at velocity U_s, while liquid drains from the bottom as a filament. Dot-dash box indicates the control volume used to derive Eq. (1): dashed box indicates the control volume used to derive Eq. (8).

1.1. Related studies

Taylor (1961) described an elegant experimental investigation of the flushing of a viscous liquid from a horizontal pipe by air. The pipe diameters were large enough (2 and 3 mm diameter) so that there were no capillary effects arising from the pressure drop across the meniscus. The slug of displacing fluid (air) left an annulus of the initial liquid in its wake. The

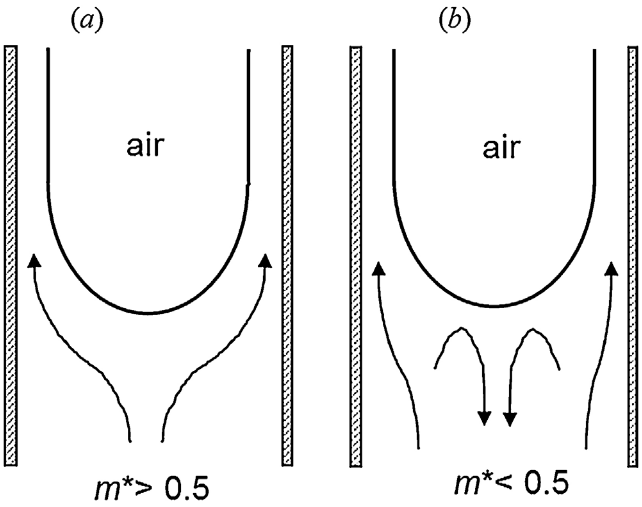

Fig. 2 – Sketches of liquid motion near nose of a slug, based on sketches in Taylor (1961). Arrows indicate motion of fluid displaced by the slug, relative to the slug nose.

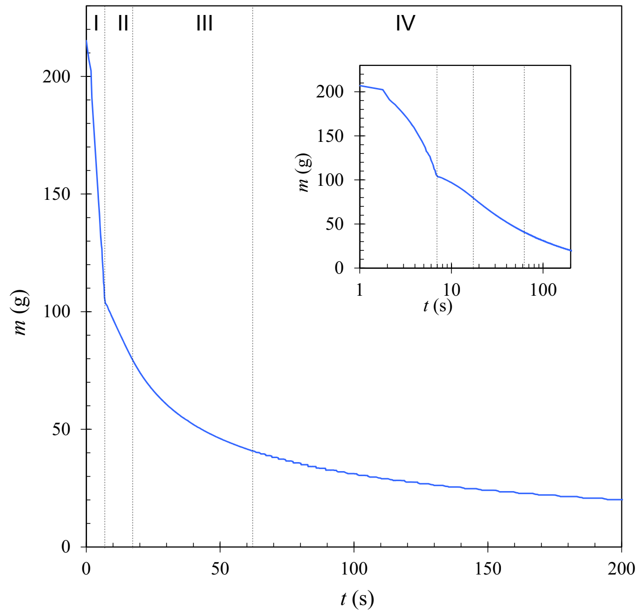

Fig. 3 – Mass of liquid remaining in tube (calculated by difference) for honey in glass tube (L = 433 mm, D = 21.7 mm; 22.5 °C). The initial mass, m_0, was measured as 225.85 g. Dashed lines show boundaries between stages. Inset shows data with time plotted on logarithmic scale.

fraction of initial liquid remaining in the pipe, which we denote m^*, was found to be determined by the dimensionless group $\mu U_s/\sigma$, where μ is the dynamic viscosity of the Newtonian liquid being flushed, U_s the slug velocity and σ the surface tension. Cox (1962) continued this work, again with Newtonian liquids, and showed that m^* initially increased with $(\mu U_s/\sigma)^{0.5}$ and approached an asymptote of 0.62 at high $\mu U_s/\sigma$.

Taylor also reported that the flow pattern in the liquid immediately ahead of the finger changed significantly around $m^* = 0.5$, as shown in Fig. 2. He stated that at $m^* = 0.5$ the flow velocity in the liquid at points ahead of the meniscus is identical to that at the meniscus, *i.e.* it is in plug flow. For $m^* < 0.5$ there is recirculation in the liquid ahead of the slug nose. We report this result because we observe in our experiments that the initial phase of drainage under gravity is associated with $m^* \geq 0.4$–0.5. For $m^* > 0.5$, liquid ahead of the meniscus flows into the film at the side of the descending slug.

We present a model, derived for Newtonian liquids such as those studied by Taylor and by Cox, which predicts the effect of experimental parameters on m^* and compare the model predictions with the results obtained with the Newtonian fluid (honey) and the non-Newtonian ones.

Following the passage of the slug of rinsing fluid, drainage involves the gravity-driven flow of the liquid film remaining on the inner wall of the tube. Self-drainage from a plane wall has been studied at length, starting with the work of Jeffreys (1930) on the dynamics of the film remaining on a flat plate as it is pulled upwards from a bath of liquid. Jeffreys' stated motivation was the drainage of liquid from the walls of cylindrical vessels and considered cases of low curvature, where the wall could be considered as a flat plate; the current work considers cases where curvature is important. These flows underpin many coating operations and have been studied for various geometries and fluid rheologies (*e.g.* White and Tallmadge, 1966; de Kee et al., 1988). More recently, Sherwood has considered the draining of fluid from the walls of process vessels of various curved shapes subject to gravity (2009) and centrifugal (2013) body forces. A model based on the approach reported by Van Rossum (1958) is shown here to give a reasonable description of drainage of the annular film formed in the later stages of the experiments with vertical tubes.

2. Modelling

The liquid leaving the tube is collected on a balance. Fig. 3 shows an example of the mass of material remaining in the tube, calculated by difference, for a typical experiment with honey. Four stages are evident, labelled as:

- *I Plug flow*
  The air slug moves downwards and the tube empties at a constant rate. Videos indicated that the nose of the slug travelled at a constant velocity, leaving an annular film of liquid behind. This stage ends when the slug reaches the bottom of the tube, at time t_I. The mass in the tube at this point is m_I and the ratio of m_I to the initial mass is denoted m^*, for comparison with the Taylor (1961) results.
- *II Second linear stage*
  In several cases, stage I was followed by a shorter period in which the drainage rate was constant. This stage ended at time t_{II} when the mass remaining in the tube was m_{II}.
- *III, IV Decreasing rate stages*
  After t_{II}, or t_I in cases where a second linear stage was not evident, the rate of drainage decreased with time. At some point the liquid ceased to drain as a steady filament and changed to a dripping regime, labelled IV. The steps in m in Fig. 3 are the result of droplet formation.

Quantitative models, based on steady state flows, are presented to describe stages I–III.

2.1. *Stage I, plug flow*

Consider the steady flow of liquid of density ρ along a tube of internal diameter R inclined at angle θ to the vertical. The wall shear stress, τ_w, matches the matches the component of the weight of the fluid in the direction of the tube axis, giving

$$\tau_w = \frac{1}{2} R\rho g \cos\theta \tag{1}$$

where g is the acceleration due to gravity. For steady laminar flow of a Newtonian fluid with viscosity μ along a tube, the wall shear stress is given by

$$\tau_w = \frac{16}{Re}\frac{\rho U^2}{2} \tag{2}$$

where Re is the Reynolds number, and U is the mean velocity of the liquid. This gives explicit results for U,

$$U = \frac{R^2}{8}\frac{\rho g \cos\theta}{\mu} \tag{3}$$

and the apparent wall shear rate, $\dot{\gamma}_{app}$

$$\dot{\gamma}_{app} = 4\frac{U}{R} = \frac{1}{2}\frac{R\rho g\cos\theta}{\mu} \tag{4}$$

Eqs. (2) and (4) are useful for determining the range of shear rates and/or shear stresses that need to be considered when determining the rheological behaviour of a non-Newtonian fluid. For the test in Fig. 3, $R \sim 0.01$ m, $\rho \sim 1415$ kg m^{-3}, $g = 9.81$ m s^{-2} and $\mu \sim 7.1$ Pa s, giving $\tau_w = 70$ Pa, $\dot{\gamma}_{app} \sim 10$ s^{-1}, $U = 24$ mm s^{-1} and $Re = 0.005$, indicating that the flows are expected to be laminar.

The volumetric flow rate, $Q_I = \pi R^2 U$, is also used as a reference flow rate:

$$Q_I = \frac{\pi R^4}{8}\frac{\rho g\cos\theta}{\mu} \tag{5}$$

For a power law fluid which exhibits Ostwald-van de Waele behaviour, *viz.*

$$\tau = K\dot{\gamma}^n \tag{6}$$

where n is the power law index and K the consistency, the corresponding result is:

$$Q_{I,PL} = \pi\rho D^{3n+1/n}\left(\frac{n}{(3n+1)}\frac{1}{8^{n-1/n}}\right)\left(\frac{g\cos\theta}{32\ \ K}\right)^{1/n} \tag{7}$$

where D is the tube diameter. These predictions for the volumetric flow rate are compared with the measured (mass) flow rates.

The finding that $m^* \approx 0.5$ suggests that this quantity can be predicted by building on the work by Taylor (1961) and Cox (1962). For steady flow in stage I, consider the control volume drawn round the slug nose shown by the dashed box in Fig. 1. Equating volumetric flows in and out gives

$$Q_A + \pi r_i^2 U_S = Q_I \tag{8}$$

where Q_A is the flow rate in an annular film with inner radius r_i. The experimental results show that the ratio of the mass remaining in the tube at the end of stage I to the initial mass, m^*, was around 0.5, giving $r_i \sim R/\sqrt{2}$. It can be shown that the local velocity, u, at radial position r in such an annulus of liquid flowing downwards under gravity is given by

$$u = \frac{\rho g R^2}{2\mu}\left(\frac{1}{2}(1-x^2) + x^2 \ln x\right) \tag{9}$$

where $x = r/R$. The volumetric flow rate in the annulus, Q_A, is given by

$$Q_A(x_i) = Q_I(1 - 4x_i^2 + 3x_i^4 - 4x_i^2 \ln x_i) \tag{10}$$

For the case where $m^* = 0.5$, $x_i = 1/\sqrt{2}$ and $Q_{II} = 0.0966\ Q_I$, or $Q_{II} \sim Q_I/10$. Combining (8) and (10) gives

$$U_s = U\frac{\pi R^2}{\pi r_i^2}(4x_i^2 - 3x_i^4 + 4x_i^2\ln x_i) = U(4 - 3x_i^2 + 4\ln x_i) \tag{11}$$

Taylor (1961) presented data relating the fraction of mass left by an air slug to the group $\mu U_s/\sigma$. His data were replotted in the form $\mu U_s/\sigma = f(x_i)$, and a third order polynomial fitted to the data (see Appendix) over the range of interest ($m^* > 0.4$), giving

$$\frac{\mu U_s}{\sigma} = f(x_i) = -797.12x_i^3 + 186.7x_i^2 - 1473.8x_i + 386.29 \tag{12}$$

Substituting for U from Eq. (3) yields

$$\frac{f(x_i)}{4 - 3x_i^2 + 4\ln x_i} = F(x_i) = \frac{R^2\rho g}{8\sigma}\cos\theta \tag{13}$$

or

$$F(x_i) = \frac{Eo}{8}\cos\theta \tag{14}$$

where Eo is the Eötvös number. It is notable that the viscosity does not appear in this relationship. The expression in Eq. (10) is unlikely to be accurate for the non-Newtonian materials, and it is of interest to compare the agreement obtained for these liquids with that for the honey, which is Newtonian.

For the parameters in this study ($0.0088\ \text{m} \le R \le 0.0217$ m, $\rho = 1330$ or 1415 kg m^{-3}; σ values in Table 3), Eo ranges from 4 to 69 for honey and 5 to 100 for the Marmite^{TM} fluids. Eq. (14) was solved numerically for the range of values of 1/8 $Eo\cos\theta$ arising in this work and m^* was then calculated using

$$m* = 1 - x_i^2 \tag{15}$$

The results are compared with the experimental values of m^* in Fig. 6.

2.2. Second linear stage, stage II

Passage of the air slug leaves an annulus of liquid behind. Measurements of the thickness of the annular film, achieved by placing a draining tube at stage II promptly in a freezer, indicated that the film was quite uniform. Drainage in the second linear stage for vertical tubes was modelled as the steady flow of an annulus of liquid with outer radius R and inner radius r_i, where r_i is the radius corresponding to the fraction of material remaining at the end of the plug flow stage, using Eq. (10).

The result for Q_A for a vertical tube ($\theta = 0$) can be compared with the flow rate estimated using the Nusselt film result (Nusselt, 1916) for a steady flow of liquid of thickness δ down a vertical wall. The flow rate per unit width of a Nusselt film

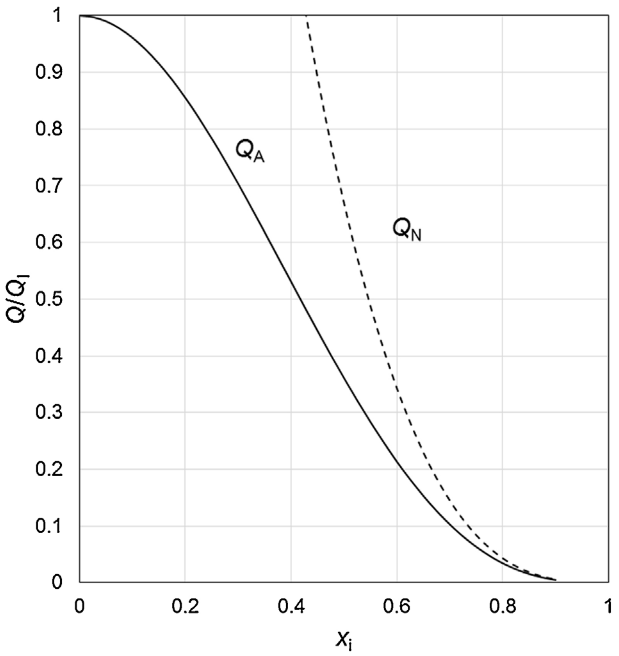

Fig. 4 – Comparison of flow rate in viscous Newtonian annular film calculated by Eq. (10), Q_A, and that estimated using the Nusselt film result, Q_N, Eq. (16). Q_I is the flow rate in a full tube, Eq. (5).

is $\rho g\delta^3/3\mu$: the flow in the annulus, Q_N, is then approximated as

$$Q_N = 2\pi R\frac{\rho g\delta^3}{3\mu} = \frac{2\pi R\rho g}{3\mu}(R-r_i)^3 \tag{16}$$

and

$$\frac{Q_N}{Q_I} = \frac{16}{3}(1-x_i)^3 \tag{17}$$

Fig. 4 compares Q_A and Q_N. The latter overpredicts the flow rate but the two expressions converge to the same result as x_i approaches unity and the effect of curvature diminishes. At $x_i \sim 1/\sqrt{2}$, $Q_A/Q_I = 0.097$ and $Q_N/Q_I = 0.134$.

Drainage at a constant rate could be expected to continue until the thinning of the annulus became significant. The time for this to occur was estimated from L/u_i, where L is the length of the tube and u_i is the velocity of the fluid at the interface when $x_i = 1/\sqrt{2}$. This gives $t_{II} - t_I = 3.26L/U$. Inspection of the data where a second linear region was observed indicated that there was no consistent trend in the duration of this second stage compared to the first: the above estimate provided an upper bound for the values of $t_{II} - t_I$, but there was considerable variation in this value (data not reported).

2.3. *Drainage with a shrinking annulus, stage III*

The viscous draining film model presented by Van Rossum (1958) was adapted to the annular geometry. The thickness of the annular film, δ, varies with axial position along the tube, z. Liquid enters a control volume drawn between z and $z+\partial z$ at flow rate Q_A: a volume balance gives

$$\frac{\partial Q_A}{\partial z} + \frac{\partial V_A}{\partial t} = 0 \tag{18}$$

where V_A is the volume of liquid in the annulus between z and $z+\partial z$. The approximation $dV_A = 2\pi R\delta\partial z$ is employed to give an analytical solution. The difference between this and the correct result $(2\pi R\delta - \pi\delta^2)\partial z$ is about 15% for the widest annulus considered here. Eq. (18) becomes

$$\frac{1}{2\pi R}\frac{\partial Q_A}{\partial z} + \frac{\partial \delta}{\partial t} = 0 \tag{19}$$

The result for Q_A, Eq. (10), does not have a simple dependency on δ so the function was fitted to a power law expression, $Q_A/Q_I = a_1(\delta/R)^\alpha$ over the range of δ values of interest ($0 < \delta/R < 0.707$), giving

$$\frac{Q_A}{Q_I} \approx 3.3936\left(\frac{\delta}{R}\right)^{2.8644} \quad R^2 = 0.9997 \tag{20}$$

For comparison, the Nusselt film result is $Q_N/Q_I = 5.33(\delta/R)^3$. Substituting (20) into (19) gives

$$\underbrace{\frac{3.3936}{2\pi}\frac{Q_I}{R^{3.8644}}}_{k}\frac{\partial \delta^{2.8644}}{\partial z} + \frac{\partial \delta}{\partial t} = 0 \tag{21}$$

Writing $\delta^{2.8644} = \delta^\alpha$, one solution, based on scaling and similarity, is

$$\delta = k \times (k\alpha)^{1/\alpha - 1}\left(\frac{z}{t}\right)^{1/\alpha - 1} \tag{22}$$

The measured quantity is the flow rate at the tube exit, Q_{III}. Setting $Q_{III} = Q_A(z=L)$ gives

$$Q_{III} = a_1 Q_I\left[\frac{\delta(z=L)}{R}\right]^\alpha = a_2\left(\frac{L}{t}\right)^{\alpha/\alpha - 1} \tag{23}$$

Writing Eq. (23) as $Q_{III} = a_3 t^\beta$, where$\beta = -1.536$, the drainage rate in stage III is given by

$$\frac{dm}{dt} = -\rho a_3 t^\beta \tag{24}$$

Integrating from $m = m_{II}$ (or m_I if there is no second linear stage) at time t_{II} (or t_I) gives

$$m = m_{II} - \frac{\rho a_3}{1+\beta}(t - t_{II})^{1+\beta} \tag{25}$$

With $\beta = -1.536$, Eq. (25) predicts $m_{II} - m(t) \propto t'^{-0.536}$, where t' is elapsed time ($t' = t - t_{II}$). It is more convenient to present the experimental results in the form $(m_{II} - m(t))^{-1.836}$ *versus* t'.

A result similar to Eq. (25) is obtained for draining of a thin annular film of thickness δ and volume $2\pi RL\delta$. If the rate of drainage per unit width is given by the Nusselt film result, *i.e.* $Q \propto 2\pi R\delta^3$, the solution is of the form δ^{-2} (and thus m^{-2}) $\propto t'$.

3. Methods and materials

3.1. *Drainage tests*

Perspex or borosilicate glass tubes were obtained with three different internal diameters and cut to give comparable *L/D* ratios, summarised in Table 1. The tubes were rinsed out with water, cleaned thoroughly with detergent solution, rinsed in hot water then dried before each test.

The mass of each tube before and after filling was measured. The bottom end of the tube was stoppered and the fluid added slowly to avoid entraining air bubbles. The tube

Table 1 – Dimensions of tubes used in drainage tests.

Material	D (mm)	L_1 (mm)	L_2 (mm)	L_3 (mm)	L_1/D (–)	L_2/D (–)	L_3/D (–)
Glass	8.8	100	200	500	11.4	22.7	56.8
	15.3	158	317	791	10.3	20.7	51.7
	21.7	217	433	1083	10.0	20.0	49.9
Perspex	7.9	100	200	500	12.7	25.3	63.3
	15.0	158	317	791	10.5	21.1	52.7
	22.0	217	433	1083	9.9	19.7	49.2

was then mounted at the desired angle to the vertical, determined using an electronic spirit level. Liquid drained into a dish located on an electronic balance connected to a datalogging PC. The response time for measuring the mass was short for steady flows. The fluids tested were not strongly viscoelastic so negative internal stresses, which could give rise to a fluid siphon effect and reduce the weight of the filament, were not expected to occur. Surface tension contributions were estimated to generate an upward force in the filament equivalent to less than 0.1 g (and would decrease steadily with filament diameter): this was considered to be a small effect.

3.2. *Test fluids*

3.2.1. *Honey*

The honey was a clear variety purchased from a local supermarket. Its rheology was studied using cone and plate tools on a Bohlin CVO 120 controlled stress device over the temperature range 15–25 °C likely to be encountered in the laboratory. The honey was Newtonian with a viscosity of approximately 8 Pa s at 21 °C. The temperature dependency fitted an Andrade relationship, *viz*.

$$\mu = 1.1 \times 10^{-13} \exp\left(\frac{8900}{T}\right) \tag{26}$$

where T is in Kelvin. The honey density was measured as $1415 \pm 10\,\mathrm{kg\,m^{-3}}$.

3.2.2. *Marmite™*

Two varieties of Marmite™ were obtained: DExtract, an intermediate from the factory line, and Squeezy, a product with a lower apparent viscosity marketed in squeezable plastic containers. The solids content of the two materials were determined by heating in an oven at 90 °C to constant residual mass, giving solids fractions of 0.731 and 0.712 for DExtract and Squeezy, respectively. The density of the materials was similar, at $1330 \pm 10\,\mathrm{kg\,m^{-3}}$. The rheology of both varieties was studied on the Bohlin device using roughened parallel plates (maximum peak height $63 \pm 10\,\mu\mathrm{m}$; Malvern Instruments, 2016) with a 1 mm gap. Cone and plate tools were not used owing to the high solids content. The solids were chiefly protein aggregates with sizes less than 1 μm. A small number salt crystals were present, with particle sizes up to 50 μm (White et al., 2008).

Increasing then decreasing shear stress ramps were imposed from (i) 10 to 100 Pa; (ii) 10 to 300 Pa; and (iii) 10 to 1000 Pa, to determine the influence of thixotropy. Each step lasted 3 s: the apparent viscosity was recorded when the strain rate reached a steady value, which took less than 3 s. The samples were left to rest for approximately 5 min after loading. Pre-shear was not applied.

The results obtained at 19 °C are summarised in Fig. 5. Both varieties show an initial increase in apparent viscosity (on the upward leg) until the shear stress reaches about 20 Pa, after which the material exhibits shear thinning. The extent of shear thinning increases with the applied shear stress. On the return (decreasing shear stress) ramp there are noticeable

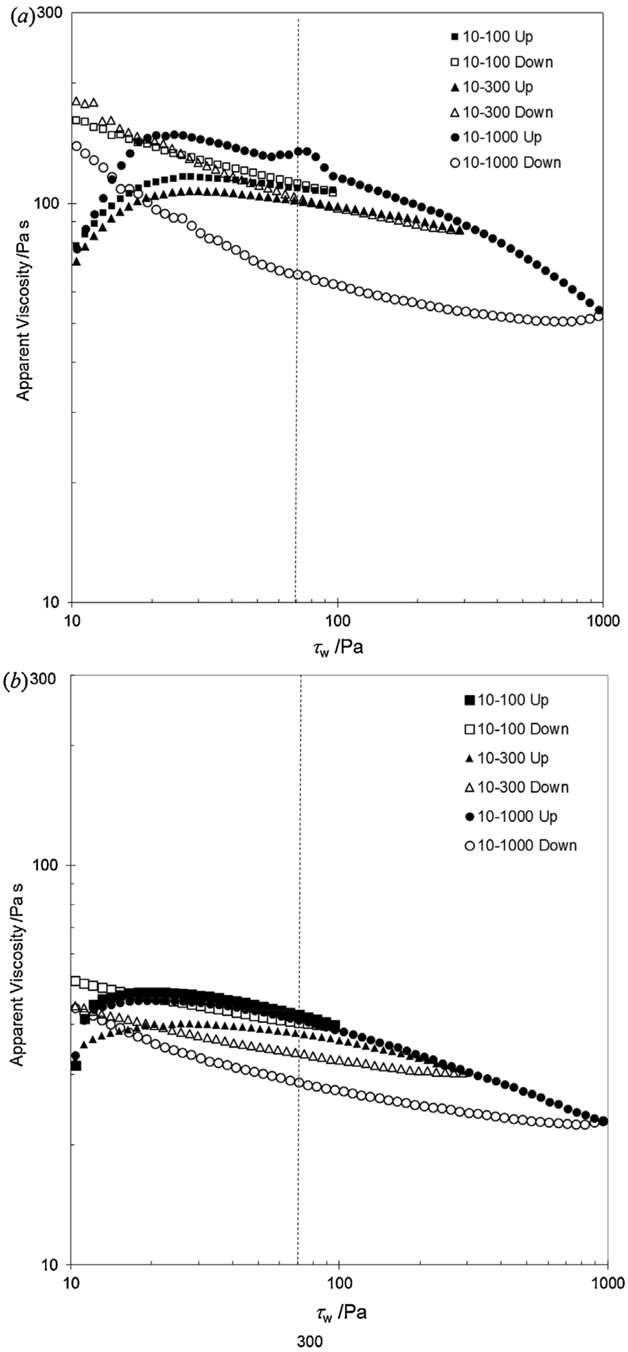

Fig. 5 – Apparent viscosity of Marmite™ fluids obtained from steady state shear stress sweeps at 19 °C. (a) DExtract, (b) Squeezy. Vertical dashed line shows upper limit of wall shear stresses calculated using Eq. (1) for the drainage tests.

Table 2 – Rheological power law model parameters for Marmite™ fluids extracted from return sweeps for $\tau_w < 100$ Pa (see Fig. 5).

	Parameter	Temperature		
		17 °C	19 °C	21 °C
DExtract	n	0.85	0.82	0.75
	K/Pa s^n	108	100	95
Squeezy	n	0.91	0.89	0.89
	K/Pa s^n	45	43	38

differences from the behaviour on the upward sweep. These differences are particularly large for samples which had been subjected to shear stresses above 100 Pa. These data confirm that both materials are thixotropic. For both materials one of the series shows a different profile for the initial ramp, even though the sample was subjected to the same loading, preshear and stress–time history. This variation illustrates the challenges in studying these complex food fluids.

For the samples sheared up to 100 Pa the difference for the Squeezy material is smaller: for both materials the return leg data could be fitted to Eq. (6) and the power law parameters thus generated are reported in Table 2. The DExtract exhibited less Newtonian behaviour (smaller n), with a larger consistency. These parameters were used to estimate the steady drainage rate using Eq. (7).

Also plotted in Fig. 5 is the largest shear stress expected to be generated in the drainage tests. At approximately 70 Pa, this lies below the range at which strong thixotropic effects were observed in the rheological tests, discussed above.

Loading the sample also subjects the sample to some shear history and the influence of the loading stage was assessed by a simple draining test. In these, the tube was half-filled with sample and stoppered at both ends. It was then inverted twice, allowing the bulk of the fluid to flow to the other end each time, then left to rest. After a rest period ranging from 30 min to 24 h, a standard draining test was conducted and the initial draining rates compared. There was no significant difference between the flow rates for tubes left for 1 h or longer after filling, so a standard waiting time of 2 h was used.

The surface tension and contact angles on each substrate were measured for each fluid using a Krüss DSA 100 goniometer. The Results in Table 3 show that the difference in contact angles on the two substrates is large for water, but small for the other fluids.

4. Results and discussion

Fig. 3 shows the mass in the tube, m, *versus* time for a test in which all four stages are evident. In first two stages, I and II, m decreases linearly with time and these are labelled the linear regions. The first linear stage was observed in all tests. The third stage, labelled III, is where annular drainage occurs at a falling rate. The final stage, IV, is where the liquid collects into droplets before falling. Cases where stage II was observed are summarised in Tables 4–6. Almost all tests showed two linear stages for a vertical pipe $\theta = 0°$, with exceptions at smaller diameters. For an inclination of 30°, two linear stages tended to be observed for longer tubes (higher L/D) – particularly with DExtract – which is attributed to the longer time for the thinning of the annular region to reach the end of the tube (see the estimate above for $t_{II} - t_I$).

For tests with DExtract and honey in the narrowest tubes, stage I was followed directly by stage IV (dropping), indicating that the rate of drainage from the annulus was insufficient to maintain a steady filament. The criterion for the filament to dropping transition represents an area for further work. Stage II was rarely observed at inclinations of 45° and 60°, which is attributed to the absence of an annular flow pattern: the drainage flow is unlikely to be axisymmetric and the shape of the interface with changes with time (see Sherwood, 2009; Ng et al., 2001). For food processing applications, tubes are likely to be vertical or horizontal: drainage from a horizontal tube

Table 3 – Surface tension and advancing contact angles on test substrates.

	Fluid			
	Honey	DExtract	Squeezy	Water
Surface tension (mN m^{-1})	72 ± 4.0	46 ± 2.1	46.9 ± 0.5	73
Contact angle				
Borosilicate glass	81° ± 5.0	49° ± 2.4	45° ± 4.3	51° ± 1
Perspex	81° ± 4.0	55° ± 3.1	54° ± 4.0	71° ± 1

Table 4 – Summary of honey drainage tests: observation of one or two linear regions. A dash indicates that this configuration was not tested.

Material	D (mm)	L (mm)	m_0 (g)	L/D (–)	Number of linear regions			
					$\theta = 0°$	$\theta = 30°$	$\theta = 45°$	$\theta = 60°$
Perspex	15	158	40	10.5	1	–	–	–
	15	317	80	21.1	2	1	1	1
Glass	8.8	100	8	11.4	2	2	1	1
	8.8	200	17	22.7	1	2	2	1
	8.8	500	43	56.8	2	2	2	1
	15.3	158	40	10.3	2	–	2	1
	15.3	317	81	20.7	2	1	1	1
	15.3	791	207	51.7	2	–	2	–
	21.7	217	107	10.0	2	1	1	1
	21.7	433	225	20.0	2	1	1	1
	21.7	1083	576	49.9	2	2	1	1

Table 5 – Summary of Squeezy drainage tests: observation of one or two linear regions. A dash indicates that this configuration was not tested.

Material	D (mm)	L (mm)	m_0 (g)	L/D (–)	Number of linear regions			
					$\theta=0°$	$\theta=30°$	$\theta=45°$	$\theta=60°$
Perspex	7.9	100	6.0	12.7	1	–	2	–
	15	158	37.0	10.5	2	2	1	1
	15	317	76.0	21.1	2	2	1	1
	22	217	105	9.9	2	1	1	1
Glass	8.8	100	8.0	11.4	1	–	1	–
	15.3	158	38.6	10.3	2	1	1	1
	15.3	317	78.0	20.7	2	2	2	1
	15.3	791	198.0	51.7	2	–	–	–
	21.7	217	105	10	2	2	1	1

with a vapour cavity into a vertical leg represents an area for future investigation.

The nature of the substrate had little influence on the observed drainage patterns. Subsequent results will show no quantitatively significant influence of substrate on drainage rates. This finding is expected, particularly for smaller angles of inclination, as dewetting (formation of dry patches) was not observed over the timescales of these tests. The following discussion focuses on drainage rates.

4.1. *Stage I – plug flow*

Fig. 6 shows that the mass remaining in the tube at the end of stage I, m^*, lay consistently around 0.5 ($\pm$0.13), for all three liquids. There is noticeable scatter but there was no clear influence of θ and D on the m^* values. High m^* values were observed with the shortest tubes when not vertical ($L/D=10$, $\theta>0$; marked on the plot) indicating that steady flow conditions may not have been achieved in these cases. There was no noticeable effect of L/D for longer tubes. This result indicates that at least half the product remaining in the tube can be recovered by waiting for an appropriate period, t_I. Discounting the outliers, the m^* values range from 0.4 to 0.52, suggesting that the flow pattern at the slug nose is expected to resemble that in Fig. 2(b).

The data for honey are plotted against the angle of inclination in Fig. 6(a) and against the dimensionless group 1/8 $Eo\cos\theta$ in Fig. 6(b). There is a weak decrease in m^* with increasing θ in Fig. 6(a), with noticeable scatter. This feature is also predicted by the model: the results for $D=8.8$ mm describe the overall trend in Fig. 6(a) but overestimate the absolute value of m^*. However, the systematic increase in m^* with increasing tube diameter predicted by the model is not present in the experimental data. When the data are plotted in the form suggested by Eq. (14), see Fig. 6(b), the model systematically overpredicts m^* for values of 1/8 $Eo\cos\theta>1/2$ (for $L/D>10$). The data distributions for Squeezy in Fig. 6(c) and DExtract in Fig. 6(d) exhibit very similar patterns: if plotted together the data overlap to a large extent (see Appendix Fig. A2). Shorter pipe lengths inclined to the vertical tend to give larger m^* values.

There is little effect of the non-Newtonian nature of the draining fluid on m^*. The data suggest that a value of 0.5 could be used to estimate the amount of product recovered, and $m^*=0.4$ could be used to estimate t_I, the time required for this to be achieved.

Fig. 7 shows the reliability of the model to predict t_I, *via* the drainage rate. The plots compare the measured mass flow rate, $\dot{m}$, measured over the stage I linear portions of the m–t profiles (see Fig. 3) to the value predicted by Eqs. (5) and (7), ρQ_I and $\rho Q_{I,PL}$, respectively, using the measured rheological parameters. There is good agreement between the measured and predicted flow rates for honey and Squeezy, *i.e.* the Newtonian and weakly shear-thinning liquid, for all values of D, L/D and θ tested. The differences that arise between measured and predicted values for Squeezy (Fig. 7(b)) are likely due to the selection of rheological model and its parameters. The DExtract results in Fig. 7(c) show a systematic difference between the model and measured flow rates. Eq. (7) tends to underpredict the experimental values and indicates that a more detailed rheological model, such as the Carreau–Yasuda model employed by White et al. (2008), should be used to estimate Q_I. The choice of rheological parameters, however, remains a challenge, as the thixotropy evident in Fig. 5 indicates that the parameters will be determined by the recent shear history of the material, particularly the rate at which it was being pumped before flow was stopped, and the length of any delay before emptying.

Table 6 – Summary of DExtract drainage tests: observation of one or two linear regions. A dash indicates that this configuration was not tested.

Material	D (mm)	L (mm)	m_0 (g)	L/D (–)	Number of linear regions			
					$\theta=0°$	$\theta=30°$	$\theta=45°$	$\theta=60°$
Perspex	7.9	100	6	12.7	1	1	–	–
	15	158	38	10.5	2	2	1	1
	15	317	76	21.1	2	2	2	1
	22	217	106	9.9	2	2	1	–
Glass	8.8	100	8	11.4	1	–	1	–
	15.3	158	38	10.3	2	2	1	1
	15.3	317	77	20.7	2	2	1	1
	15.3	791	196	51.7	2	–	–	–
	21.7	217	107	10	2	2	1	1

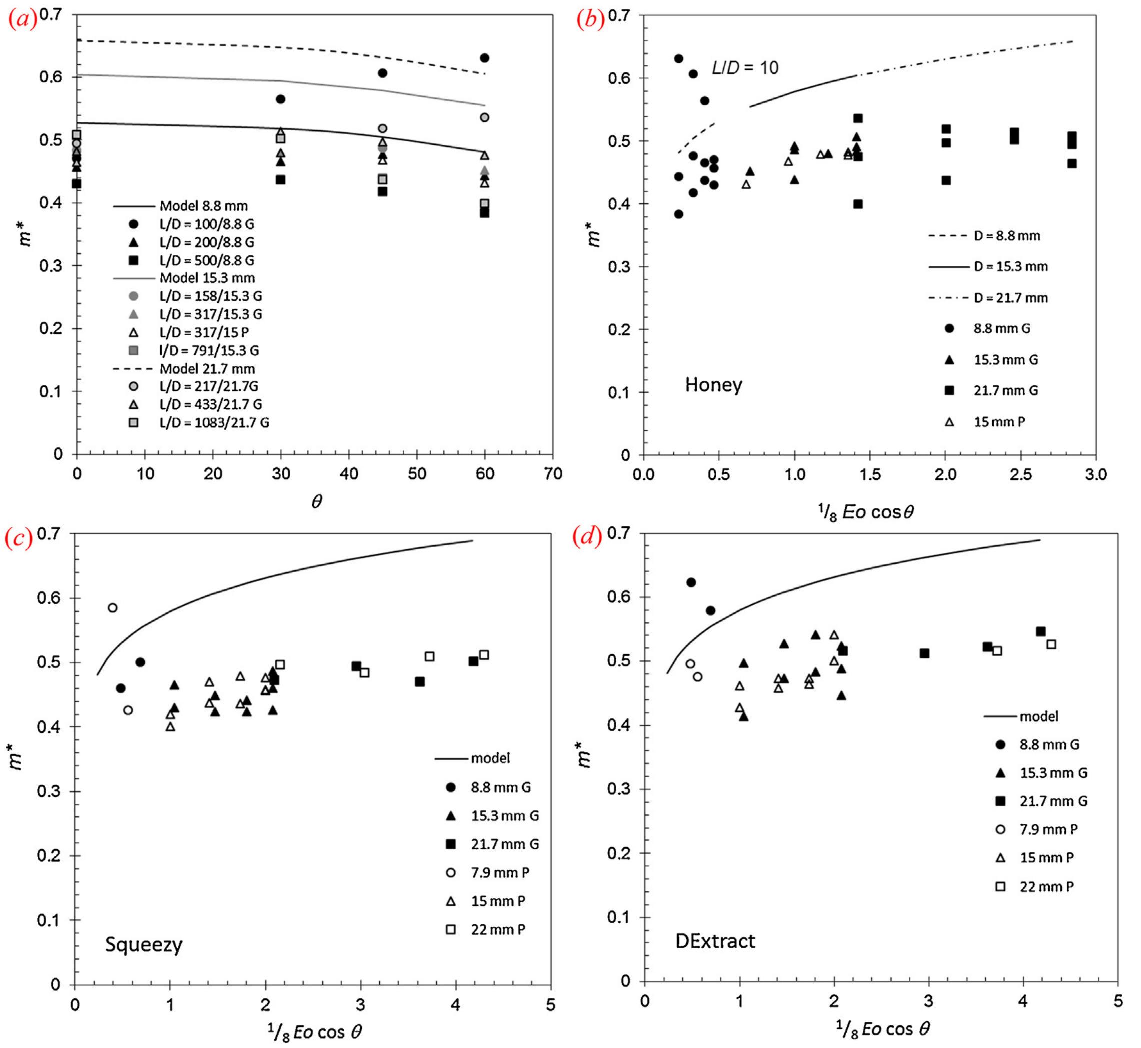

Fig. 6 – Mass fraction remaining at end of stage I, m^*. (a) Honey, showing effect of angle of inclination; (b) honey data, plotted against 1/8 $Eo\cos\theta$; (c) Squeezy; (d) DExtract. Open symbols – Perspex; solid symbols – glass. Error bars are smaller than symbols. Loci show model predictions for each case.

In the absence of a reliable *a priori* prediction of mass flow rate for rheologically complex materials such as DExtract, the effect of pipe inclination was tested by comparing the ratio of the mass flow rates of the vertical and inclined cases suggested by Eq. (7), namely

$$\left.\frac{\dot{m}_{\mathrm{I}}(\theta)}{\dot{m}_{\mathrm{I}}(\theta=0)}\right| = (\cos\theta)^{1/n} \qquad (27)$$

The DExtract data in Fig. 7(c) are plotted in this form in Fig. 8, using the n values in Table 2. The data exhibit the expected trend, with noticeable scatter. This result indicates that the dependency of the flow rate on the wall shear stress (which is proportional to $g\cos\theta$, Eq. (1)) is not modelled reliably by Eq. (7): the trend is captured but the absolute value of $Q_{\mathrm{I,PL}}$.

4.2. *Stage II – second linear stage*

The analysis of a falling annular Newtonian film, Eq. (10), predicts that for vertical tubes $\dot{m}_{\mathrm{II}}/\dot{m}_{\mathrm{I}}{\sim}0.1$. For vertical tubes ($\theta=0°$), the ratio was around 0.1 for all three fluids, despite the differences in rheology. Fig. 9 presents the ratio of the two flow rates for most of the tests where a second linear stage was observed (see Tables 4–6): the angle is plotted as $\cos\theta$, to capture the influence of gravity. In all cases, $\dot{m}_{\mathrm{II}} < \dot{m}_{\mathrm{I}}$. The ratio decreases with increasing $\cos\theta$ (decreasing angle of inclination), which reflects the increase in $\dot{m}_{\mathrm{I}}$ with $\cos\theta$. The variation in the data increases with angle of inclination (smaller $\cos\theta$). This is likely to arise from the change in flow pattern in stage II from a concentric annulus to a stratified flow as the angle of inclination increases: the flow pattern will be determined by surface tension (and Bond number) as well as the rheology of the fluid.

4.3. *Stage III – falling rate regime*

Examples of data collected in stage III are presented in the form suggested by Eq. (25), $\Delta m^{-1.8644}$ *versus* t', in Fig. 10. For honey there is good agreement with the model trend over the first 100 s, shown by the inset on the figure, by which point $\Delta m^{-1.8644}$ is approximately 60 $g^{-1.8644}$. Similarly linear behaviour is evident up to 60 $g^{-1.8644}$ for the Squeezy and DExtract cases, but these fluids require longer times, of around 2000 and 8000 s, respectively. The longer times required for DExtract and Squeezy is consistent with their higher apparent viscosity as well as their shear thinning

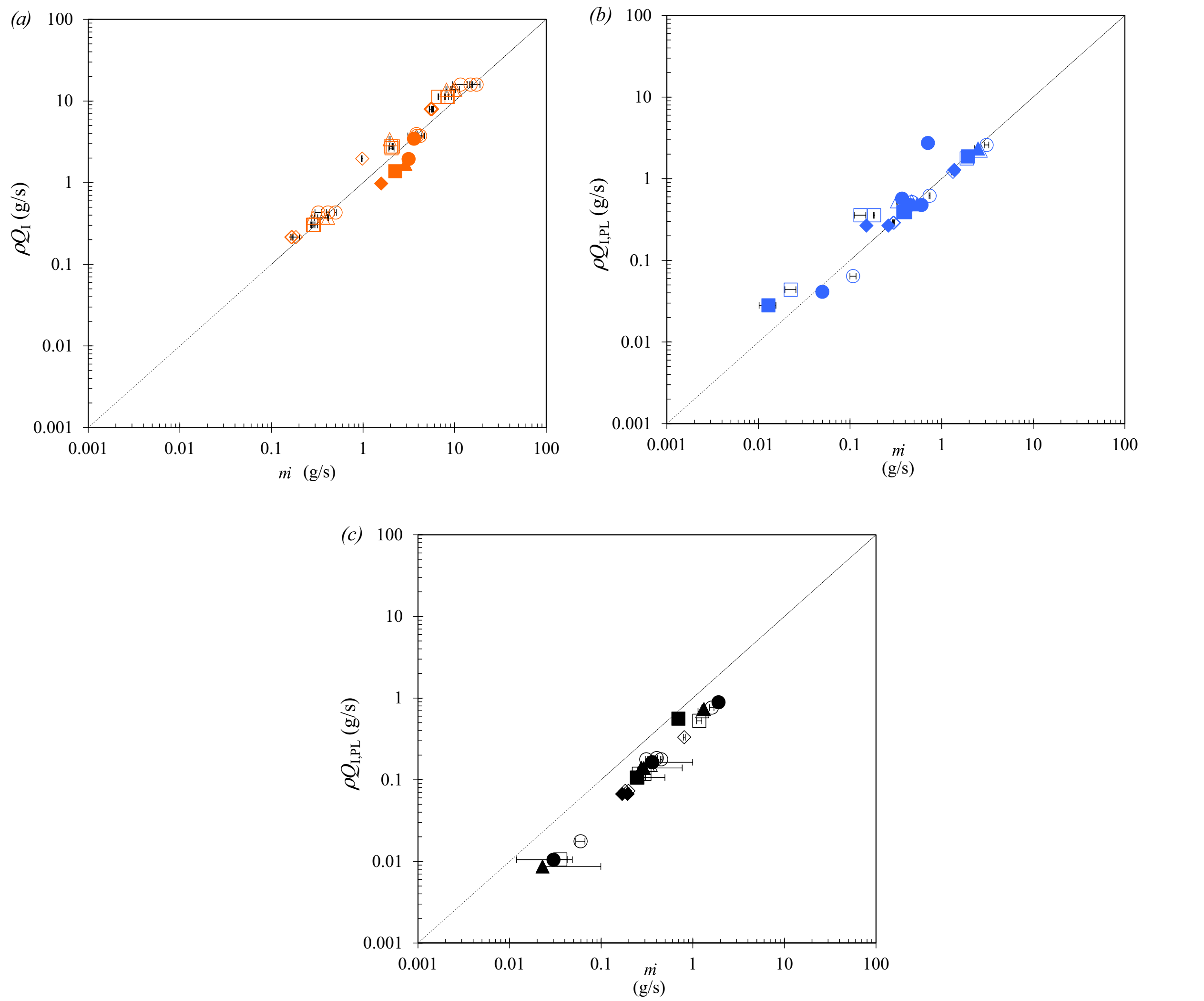

Fig. 7 – Agreement between measured and predicted mass flow rates in region I for (a) honey (ρQ_I, Eq. (5)); (b) Squeezy, (c) DExtract (both $\rho Q_{I,PL}$ Eq. (7)). Open symbols – Perspex; solid symbols – glass. Symbol shape indicates angle of inclination: ○ – 0°; △ – 30°; □ – 45°; ◇ – 60°. Error bars represent 95% confidence intervals. Dashed (diagonal) locus shows the line of equality ($y = x$).

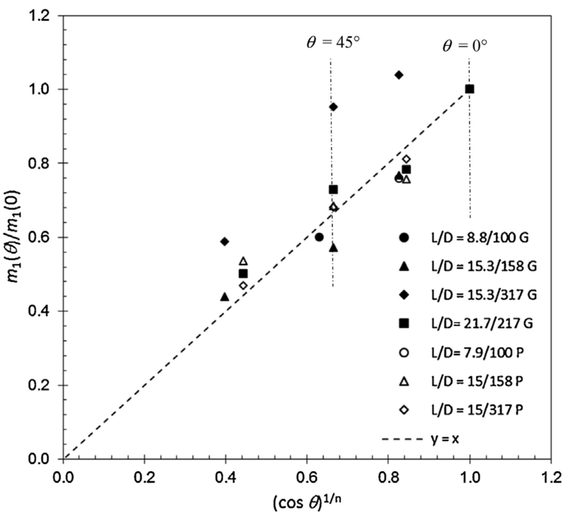

Fig. 8 – Effect of angle of inclination on drainage rate of DExtract in stage I. DExtract data in Fig. 7(c) expressed as the ratio of the drainage rate at angle θ to the vertical case ($\theta = 0$). Open and solid symbols denote tests using Perspex and glass, respectively.

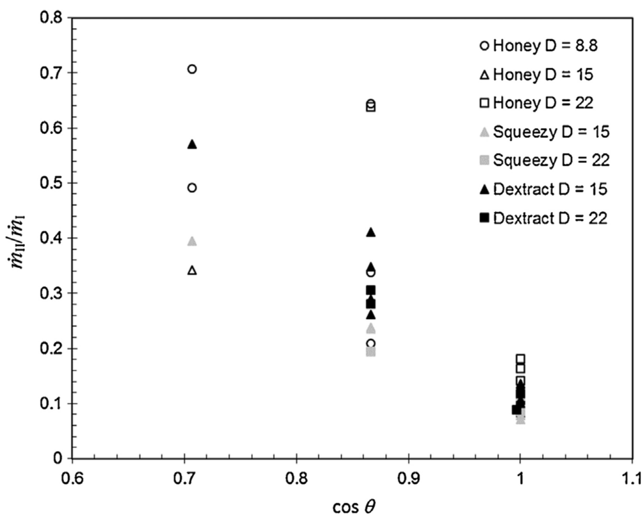

Fig. 9 – Effect of angle of inclination, expressed as cos θ, on ratio of measured mass flow rates in linear regions I and II, $\dot{m}_{II}/\dot{m}_I$. Open symbols – honey; grey symbols – Squeezy; black symbols – DExtract. Symbol shape indicates diameter (see legend).

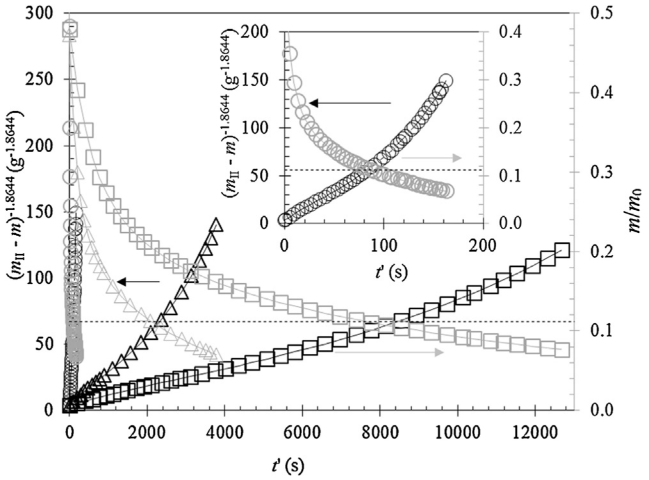

Fig. 10 – Evolution of mass remaining in tube during Stage III. $L/D = 433/21.5$, $\theta = 0°$. Grey symbols – mass fraction; black symbols, data plotted in the form suggested by Eq. (25). Circles – honey, inset shows detail of first 200 s where Eq. (20) describes the honey data; triangles – Squeezy; squares – DExtract. Dashed horizontal line indicates limit of linear behaviour for honey.

nature: their apparent viscosity is expected to increase as the film thickness (and shear stress) decreases.

4.4. *Stage IV – drop regime*

At the end of this period, at which drainage switched to drop behaviour (stage IV), the mass fraction in the tube (m/m_0) ranged from 0.11 to 0.13. Tests with the more viscous liquids were often curtailed before this point was reached. Most of the experiments gave good agreement with the model to x_i values around 0.9. Drop formation was observed at $0.91 < x_i < 0.93$ for all but the narrowest tubes.

The above results suggest that the model captures the drainage behaviour. The agreement found for Squeezy and DExtract was surprising as the model assumes Newtonian behaviour, which was not observed in the rheometry testing and the estimation of the flow rate in stage I. The degree to which these fluids can be treated as pseudo-Newtonian in this thin film drainage regime represents a topic for further investigation. Further evidence suggesting that Eq. (20) should be treated as a semi-empirical result is that the values of a_3 (Eq. (24)) obtained from fitting the experimental data did not agree with the value calculated using the properties for honey and the test geometry. The mismatch ranged from a factor of 2–500 across the configurations studied. This is not unexpected as there are several approximations made in the model, including the estimate of the film volume. The boundary conditions are unlikely to match those encountered in practice in moving from Stages I to III: this is only likely to be overcome by a detailed numerical model which calculates the flow (and evolution of film thickness) at every location.

4.5. *Application*

The aim of this investigation was to determine the feasibility of including a self-draining step into a cleaning protocol in order to increase the amount of product recovered and reduce subsequent contamination of the cleaning solutions. The results show that around 50% of the material is removed

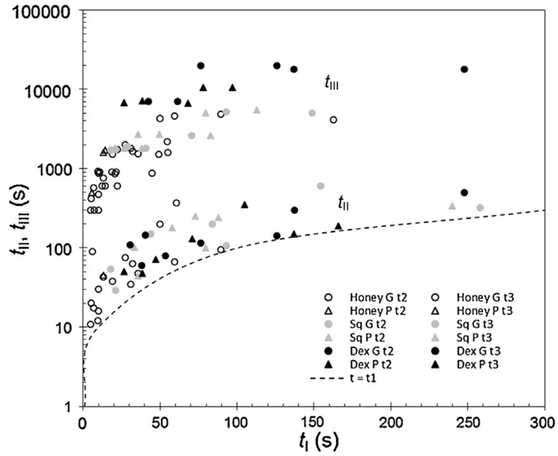

Fig. 11 – Comparison of drainage times. Symbols: open – honey; grey – Squeezy; black – DExtract: circles – glass, triangles – Perspex. Dashed line shows locus for $t = t_I$.

in stage I, with the model giving a reasonable estimate of the waiting time. More material can be recovered by waiting longer, but the rate decreases significantly after t_I. The existence of a second linear stage is related to the angle of inclination and length, with more vertical and longer pipes favouring this behaviour. The accuracy of the models to predict the flow rate in stage II is reasonable for vertical pipes but has not been explored further here. Likewise, a model for stage III drainage has been proposed, which describes the observed behaviour up to 90% removal. Its predictive accuracy, even for the Newtonian fluid tested, is poor.

Fig. 11 puts these results into perspective. After time t_I around 50% of the fluid has been removed from the pipe: t_I depends on its configuration and the fluid rheology. Where stage II is observed, a further 10% or so drains off after waiting until t_{II}, which is several times t_I: clearly, there is a diminishing return. This is confirmed by the t_{III} values, which range from 10 to 100 × t_I in achieving 80–90% removal. In a processing unit, waiting for over an hour may be acceptable but this will depend on the application and nature of the product. *A priori* prediction of t_{III} is not achievable with the models presented here.

4.6. *Evaluating a delay stage*

For a vertical pipe of length L, the time taken for 50% of the fluid to drain, t_{50}, can be estimated from $t_{50} \approx L/U$. From Eq. (3),

$$t_{50} \approx \frac{8L}{R^2}\frac{\mu}{\rho g} \tag{28}$$

Consider a 10 m length of 50 mm i.d. pipe initially filled with the honey used in this work ($\mu = 8$ Pa s, $\rho = 1415$ kg m^{-3}). Eq. (28) gives $t_{50} = 74$ s, suggesting that 50% of the product could be recovered by waiting for 2 min, say, before starting the cleaning-in-place (CIP) system. This is short compared to standard food industry cleaning cycle times. The Marmite™ varieties would require longer periods.

The prospective financial return could be estimated by comparing the cost of extra equipment required to add the step (valves, tankage, pump and time spent reprogramming the control system) against the savings incurred. The latter would include

(i) The value of product recovered rather than being purged with the initial CIP rinse.

(ii) The reduction in energy and chemicals required for cleaning, related to there being less product to remove from the pipe.
(iii) The reduction in volume of aqueous effluent sent for waste treatment. For the fluids studied here, the volumes of water can be considerable. The honey, with a high sugar content, generates waste with a high biological oxygen demand. Likewise, Marmite™ has a high salt content and the CIP waste water must be diluted or treated in order to reach discharge limits.

These costs are all likely to be site specific and all depend on the frequency with which the line is cleaned.

4.7. *Non-Newtonian fluids*

Where the process is able to accommodate long drainage times, the fluid is likely to be viscous and non-Newtonian, like the DExtract and Squeezy fluids employed in this work. Both DExtract and Squeezy demonstrated thixotropy. This introduces challenges into modelling, some of which have been mentioned above. The rheological results (Fig. 5) indicated that this would have noticeable effects when the wall shear stress exceeded 100 Pa, which was not encountered in these tests. Commercial lines are likely to employ larger pipes: for example, a vertical 50 mm i.d. line would give a wall shear stress of 160 Pa for DExtract. The apparent viscosity is then expected to be smaller and the drainage times shorter. Moreover, the liquid is likely to have been pumped in the period prior to drainage, subjecting it to an even higher wall shear stress, and will exhibit, again, a lower apparent viscosity. Selection of the rheological model and parameters for use in the drainage calculation in this case requires careful consideration.

5. Conclusions

The self-drainage of three food-related viscous liquids from circular pipes was investigated in experiments featuring different pipe diameters, lengths and angles of inclination to the vertical. The mass of fluid remaining in the pipe was measured. Drainage exhibited an initial stage characterised by a constant drainage rate, during which the volume of material in the pipe decreased by about 50%. Thereafter drainage could follow a second constant rate regime, a falling rate regime and one characterised by drop formation, depending on the pipe configuration and nature of the fluid. The nature of the pipe wall did not have a significant effect on drainage behaviour.

Quantitative models for the rate and extent of drainage in the initial stage were developed. The former gave reasonable estimates of the drainage rate while the latter tended to over-predict the fraction of material remaining in the tube at the end of the initial stage. Whereas the rate was strongly affected by the rheology of the fluid, the rheology had little influence on the fraction remaining: further work is required to allow this to be predicted reliably. Similarly, models for the drainage rate in the second and third stages offered insight into the behaviour but were not able to predict the rates reliably.

The DExtract and Squeezy materials studied are complex fluids. They exhibited noticeable thixotropy but the models developed, particularly for the initial stage, gave reasonable estimates of their behaviour.

There is significant difference in the times required to remove 50% and 90% of the product. This suggests that partial recovery of material by self-drainage is feasible: the extended period required to remove 90% of the product may not be practicable.

Acknowledgements

Samples of Marmite™ were provided by Unilever. The data in Fig. A1 of the Appendix were extracted by Ole Mathis Magens. An EPSRC studentship for AA, supported by Procter & Gamble, is gratefully acknowledged, as are helpful discussions with Dr. David Scott.

Open Data

This article is published under Open Access with EPSRC support. The accompanying data are available at https://www.repository.cam.ac.uk/handle/1810/254584.

Appendix.

In the experiments reported by Taylor (1961), air was forced through tubes filled with viscous liquid at set flow rates. U_s and m were measured. His Fig. 2 presented measurements of

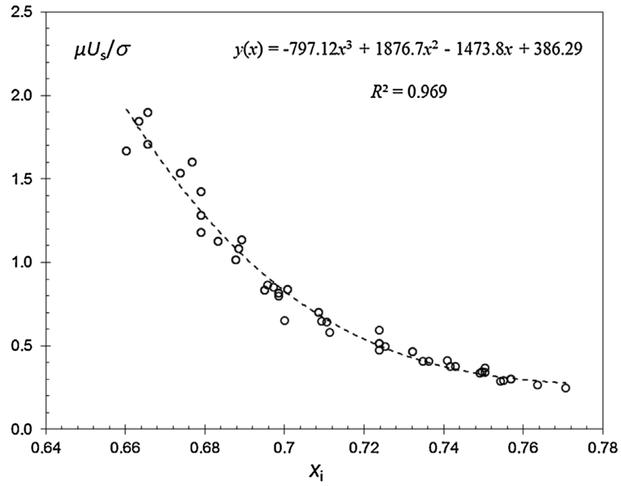

Fig. A1 – Experimental data from Taylor (1961, Fig. 2) replotted in the form $\mu U_s/\sigma = f(x_i)$. Dashed locus shows line of best fit obtained by linear regression to a third order polynomial using Microsoft Excel™.

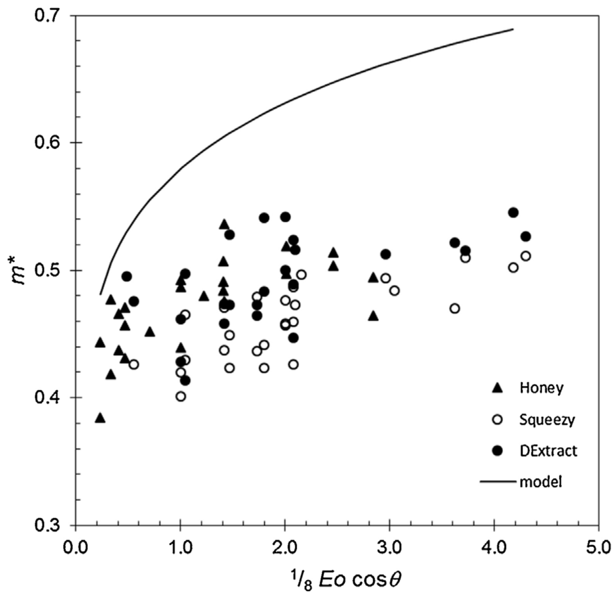

Fig. A2 – Composite plot of data from Fig. 6(b)–(d) for L/D > 10.

m^* against $\mu U_s/\sigma$: m^* was used to calculate x_i using Eq. (15) and the data are replotted in Fig. A1 as $\mu U_s/\sigma = f(x_i)$.

References

Cox, B.G., 1962. On driving a viscous fluid out of a tube. J. Fluid Mech. 14, 81–96.

Cragnell, C., Hansson, K., Andersson, T., Jonsson, B., Skepo, M., 2014. Underlying mechanisms behind adhesion of fermented milk to packaging surfaces. J. Food Eng. 130, 52–59.

de Kee, D., Schlesinger, M., Godo, M., 1988. Postwithdrawal drainage of different types of fluids. Chem. Eng. Sci. 43 (7), 1603–1614.

Fan, M., Phinney, D.M., Heldman, D.R., 2015. Effectiveness of rinse water during in-place cleaning of stainless steel pipe lines. J. Food Sci. 80 (7), 1490–1497.

Jeffreys, H., 1930. The draining of a vertical plate. Math. Proc. Camb. Philos. Soc. 26, 204.

Loibl, F., Schmidt, M.C., Auer-Seidl, A., Kirchner, C., Holtz, C., Miiller, K., Stramm, C., Langowski, H.-C., 2012. The emptying behaviour of highly viscous liquids. Part II: Development of test methods and evaluation of untreated and coated film. J. Adhes. Sci. Technol. 26, 2469–2503.

Malvern Instruments (2016). Personal Communication, 15 February 2016.

Mickaily, E.S., Middleman, S., 1993. Hydrodynamic cleaning of a viscous film from the inside of a long tube. AIChE J. 39 (5), 885–893.

Ng, T.S., Lawrence, C.J., Hewitt, G.F., 2001. Gravity-driven laminar flow in a partially-filled pipe. Chem. Eng. Res. Des. 79, 499–511.

Nusselt, W., 1916. Oberflachen kondensation des Wasserdampfes. Zeitschrift Verein Deutscher Ingenieure 60, 569–575, 541–546.

Palabiyik, I., Olunloyo, B., Fryer, P.J., Robbins, P.T., 2014. Flow regimes in the emptying of pipes filled with a Herschel-Bulkley fluid. Chem. Eng. Res. Des. 92, 2201–2212.

Sherwood, J.D., 2009. Optimal shapes for best draining. Phys. Fluids 21, 113102.

Sherwood, J.D., 2013. Optimal shapes for best centrifugal draining. Eur. J. Mech. B: Fluids 37, 124–128.

Taylor, G.I., 1961. Deposition of a viscous fluid on the wall of a tube. J. Fluid Mech. 10, 161–165.

Taylor, J.E., Van Damme, I., Johns, M.L., Routh, A.F., Wilson, D.I., 2009. Shear rheology of molten crumb chocolate. J. Food Sci. 74 (2), E55–E61.

Van Rossum, J.J., 1958. Viscous lifting and drainage of liquids. J. Appl. Res. A7, 121–144.

White, D.A., Tallmadge, J.A., 1966. A theory of withdrawal of cylinders from liquid baths. AIChE J. 12 (2), 333–339.

White, D.E., Moggridge, G.D., Wilson, D.I., 2008. Solid–liquid transitions in the rheology of a structured yeast extract paste, Marmite™. J. Food Eng. 88, 353–363.